

<https://helda.helsinki.fi>

þý Last Interglacial Climate in Northern Sweden In Speleothem Record

Finné, Martin

Multidisciplinary Digital Publishing Institute
2019-08-20

Finné, M.; Salonen, S.; Frank, N.; Helmens, K.F.; Schröder-Ritzrau, A.; Deininger, M.;
þý Holzkämper, S. Last Interglacial Climate in Northern Sweden Insights
Record. Quaternary 2019, 2, 29.

<http://hdl.handle.net/10138/348549>

Downloaded from Helda, University of Helsinki institutional repository.


This is an electronic reprint of the original article.

This reprint may differ from the original in pagination and typographic detail.

Please cite the original version.

Article

Last Interglacial Climate in Northern Sweden—Insights from a Speleothem Record

Martin Finné ^{1,2,*} , Sakari Salonen ^{3,4}, Norbert Frank ⁵, Karin F. Helmens ^{2,6}, Andrea Schröder-Ritzrau ⁵, Michael Deininger ⁷ and Steffen Holzkämper ^{2,8}

¹ Department of Archaeology and Ancient History, Uppsala University, Box 626, SE-75126 Uppsala, Sweden

² The Bolin Centre for Climate Research, Stockholm University, SE-10691 Stockholm, Sweden

³ Department of Geosciences and Geography, University of Helsinki, PO Box 64, FI-00014 Helsinki, Finland

⁴ Environnements et Paléoenvironnements, Océaniques et Continentaux, UMR 5805, Université de Bordeaux, 33615 Pessac CEDEX, France

⁵ Institute of Environmental Physics, Heidelberg University, D-69120 Heidelberg, Germany

⁶ Värriö Research Station, Institute for Atmospheric and Earth System Research INAR/Physics, University of Helsinki, P.O. Box 64, FI-00014 Helsinki, Finland

⁷ Institute of Geosciences, Johannes Gutenberg University Mainz, D-55128 Mainz, Germany

⁸ Department of Physical Geography, Stockholm University, SE-10691 Stockholm, Sweden

* Correspondence: martin.finne@antiken.uu.se; Tel.: +46-(0)18-4716238

Received: 29 June 2019; Accepted: 13 August 2019; Published: 20 August 2019



Abstract: Continental records with absolute dates of the timing and progression of climatic conditions during the Last Interglacial (LIG) from northern Europe are rare. Speleothems from northern Europe have a large potential as archives for LIG environmental conditions since they were formed in sheltered environments and may be preserved beneath ice sheets. Here, we present $\delta^{13}\text{C}$ and $\delta^{18}\text{O}$ values from speleothem Kf-21, from Korallgrottan in Jämtland (northwest Sweden). Kf-21 is dated with five MC-ICPMS U-Th dates with errors smaller than ~ 1 ka. Kf-21 started forming at ~ 130.2 ka and the main growth phase with relatively constant growth rates lasted from 127.3 ka to 124.4 ka, after which calcite formation ceased. Both $\delta^{13}\text{C}$ and $\delta^{18}\text{O}$ show rapid shifts but also trends, with a range of values within their Holocene counterparts from Korallgrottan. Our results indicate an early onset of the LIG in northern Europe with ice-free conditions at ~ 130 ka. Higher growth rates combined with more negative $\delta^{18}\text{O}$ values between ~ 127.3 and 126.8 ka, interpreted here as warmer and more humid conditions, as well as indications of a millennial-scale cold spell centered at 126.2 ka, resemble findings from speleothem records from other parts of Europe, highlighting that these were regional scale climatic patterns.

Keywords: Last Interglacial (LIG); speleothem; stable carbon and oxygen isotope compositions; climate variability; Scandinavia; Sweden

1. Introduction

The timing of the Last Interglacial's (LIG) inception has been actively studied for decades (e.g., [1–3]), as well as, in connection with it, the role of different drivers of interglacial climate. Large efforts have also been made towards answering the question of whether the climate during the LIG was overall stable or, alternatively, disrupted by spells of cold, warm, or dry climate (e.g., [4–6]). An underlying motivation is to understand the timing and progression of a warm period uninfluenced by human activity and to draw parallels between LIG with Holocene climates with regard to the strength of positive feedback mechanisms [7–9].

Speleothems can serve as climate archives even at high altitudes and latitudes where terrestrial sedimentary records of the LIG are often missing or are fragmented due to later glacial erosion during

the Last Ice Age [10,11]. In general, their growth requires the presence of liquid water, i.e., carbonate formation is proof for temperatures above the freezing point in the cave environment. The carbon and oxygen isotope profiles along the growth axis can be interpreted in terms of changes in ambient temperature and precipitation conditions, atmospheric circulation patterns and vegetation coverage above the cave (e.g., [12–14]). Speleothems are datable with high precision, with dating errors typically around a few hundred years for LIG samples, and the achievable temporal resolution can reach a few decades (e.g., [15]), thus enabling the detection and characterization of abrupt environmental events and transitions.

A further application of speleothems is as foundations of regional chronological frameworks for the LIG. Absolutely dated proxies for climate and environmental change during the LIG from the northern high latitudes are still rare. Presently, there are some carbon and oxygen isotope composition records from speleothems collected in caves in northern Norway, dated using uranium series technique, that reach back to the LIG or further [16–18]. Marine sediments have been studied in great detail but generally suffer from relatively low temporal resolution, and the chronology is often derived from comparisons with other archives and from orbital forcing models [10]. Terrestrial archives from northern Europe include lake sediments and peat sequences; however, many of them were erased through glacial erosion during the Weichselian glaciation [11]. Similarly to marine sediments, it is problematic to provide absolute chronologies for lacustrine sediments or peat sequences from the LIG period primarily because this period is beyond the limit of radiocarbon dating. A high-resolution, comprehensive environmental and climate record of the LIG has recently been obtained from lake sediments at Sokli in northeastern Finland [19–22]; however, this sequence relies on optically stimulated luminescence (OSL) dates and, thus, similar to most sedimentary records of the LIG, has no detailed, independent chronology. Because of their unparalleled absolute chronologies during the LIG, speleothem paleo-environmental records are increasingly employed as alignment targets, and thus also as sources of chronologies, for both terrestrial and marine sedimentary records [10,22]. Therefore, speleothems from Northern Europe have a large potential as archives for LIG environmental conditions since they were formed in sheltered environments and could therefore be preserved even beneath glaciers and ice sheets.

Here, we present an absolutely dated speleothem, Kf-21, from northwestern Sweden as an archive for the timing and duration of temperature conditions during the LIG that enabled speleothems to form. Comparisons of the growth period of Kf-21 with other terrestrial and marine climate archives from the Arctic and central Europe reveal a consistent picture of climatic progression with rather synchronous changes at middle and high northern latitudes. The carbon and oxygen isotope composition record with ~70-year resolution facilitates a comparison of climate development and warm/cold events with nearby sites and may serve as a dating tool for other high-resolution archives that lack precise absolute dates.

2. Study Site

Korallgrottan (64.89° N, 14.16° E, 540–600 m a.s.l.) in northern Jämtland is the largest known cave in Sweden (Figure 1), with approximately 5.5 km of passages (for details see, e.g., [23]). Korallgrottan, situated in the Caledonian mountain range, formed in a 200 to 300 m wide belt of limestone or marble (Bjurälvs limestone) of late Proterozoic to early Paleozoic age with a high calcite content (98.9%) [24,25]. The bedrock surface above the cave is overlain by a 30–50-cm-thick soil cover. The vegetation above the cave is rich in herbs, grass, and mosses but also consists of sparse forest with old spruce and birch. At nearby meteorological stations, mean annual precipitation for the reference period of 1961–1990 was 866 mm (Ankarvattnet, 4 km southeast of the cave) and annual mean temperature was 1.4 °C (Gäddede, 50 km south of the cave) [26]. From November to April, most of the precipitation falls as snow, and the snow cover generally lasts until May.

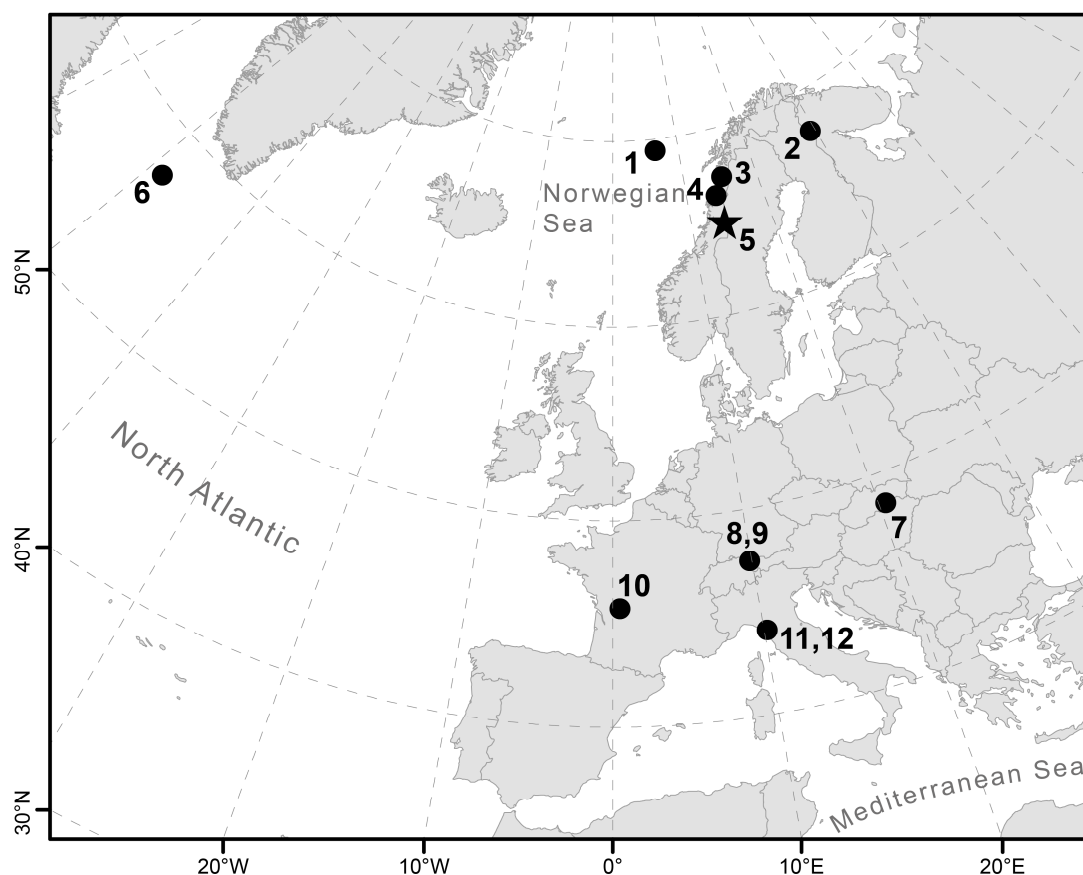


Figure 1. Map showing the location of Korallgrottan (#5, marked by a star) and sites mentioned in the text. 1: PS1243 [27,28]; 2: Sokli [19,22,29]; 3: Okshola Cave [17]; 4: Hamarnes Cave [18]; 5: Korallgrottan (this study); 6: MD03-2664 [30]; 7: Baradla Cave [31]; 8: Schneckenloch Cave [32]; 9: Hölloch Cave [32]; 10: Bourgeois-Delaunay Cave [33]; 11: Corchia Cave [34–36]; 12: Tana che Urla Cave [37].

3. Materials and Methods

Sample Kf-21 was collected in Korallgrottan in 2011. Upon collection, Kf-21 was chipped off from a larger flowstone sheet that was lodged between two boulders in the cave passage. Kf-21 is thus likely a flowstone, and its original growth position remains unknown. A chamber located in the vicinity of the collection place is located ~15 m below the surface [14]. The upper part of Kf-21 consists of dense opaque white calcite alternated with bands of clearer calcite. The bottom section displays a more complex pattern of calcite layers with wavy patterns, which formed on top of a bottom-bed consisting of rather straight and easily distinguishable layers with a total thickness of ~4 mm. The total thickness of Kf-21 is approximately 86 mm (Figure 2).

The chronology of stalagmite Kf-21 was established by U-Th dating using thermal ionization mass spectrometry (TIMS), and later complemented by multi-collector inductively coupled plasma mass spectrometry (MC-ICPMS). First, the TIMS ages were obtained in 2011 with a sample width of 7 to 10 mm in the growth direction. The samples were drilled (diameter 8 mm, borehole depth 6 mm) or cut.

For the MC-ICPMS analyses measured in 2017, much less material was needed. Approximately 100 mg powder was drilled out of the flowstone along visible growth bands, or small slabs were cut with a band saw. Samples for the MC-ICPMS analysis have a sample width of 1–2 mm. As a result, the samples represent averages over different time periods; in particular, TIMS samples integrate on average 5 times longer growth periods compared to MC-ICPMS samples.

Table 1. Results of U-series analysis for Kf-21.

IUP LAB ID_year	Mass Spec	Dft (mm)	Age * (ka)	Age ** (ka)	²³⁸ U (ng/g)	²³² Th (ng/g)	²³⁰ Th/ ²³⁸ U AR	²³⁰ Th/ ²³² Th AR	δ ²³⁴ U (‰)	δ ²³⁴ U _{initial} (‰)
5550_2011	TIMS	4.0	122.2 ± 1.6	122.1 ± 1.7	746.5 ± 1.5	4.428 ± 0.022	1.0035 ± 0.0071	517.0 ± 4.4	424.3 ± 4.0	599.1 ± 5.3
8846_2017	MC-ICPMS	7.0	124.72 ± 0.43	124.61 ± 0.39	806.348 ± 0.034	5.0698 ± 0.0076	1.0408 ± 0.0017	507.3 ± 1.1	455.8 ± 1.0	648.2 ± 1.6
8755_2017	MC-ICPMS	15.0	126.18 ± 0.58	126.05 ± 0.57	652.44 ± 0.21	4.7223 ± 0.0093	0.9664 ± 0.0021	405.4 ± 1.2	353.5 ± 1.4	504.8 ± 2.2
5551_2011	TIMS	30.5	125.5 ± 1.6	125.2 ± 1.6	492.46 ± 0.98	8.147 ± 0.030	0.8560 ± 0.0055	440.1 ± 6.8	218.7 ± 3.5	311.6 ± 4.6
8754_2017	MC-ICPMS	43.9	127.77 ± 0.83	127.43 ± 0.78	791.827 ± 0.035	13.664 ± 0.056	0.8806 ± 0.0029	156.91 ± 0.83	238.01 ± 0.95	341.2 ± 1.5
5552_2011	TIMS	67.2	128.2 ± 1.5	127.7 ± 1.4	1199.7 ± 1.2	27.33 ± 0.11	0.9010 ± 0.0054	158.1 ± 1.1	263.0 ± 2.4	377.3 ± 3.3
8823_2017	MC-ICPMS	71.0	128.63 ± 0.52	126.97 ± 0.99	1976.45 ± 0.13	155.60 ± 0.28	0.8511 ± 0.0018	33.067 ± 0.091	197.34 ± 0.62	282.5 ± 1.2
8752_2017	MC-ICPMS	73.7	130.97 ± 0.42	130.17 ± 0.66	1639.955 ± 0.064	63.425 ± 0.087	0.8686 ± 0.0015	68.31 ± 0.15	208.48 ± 0.62	301.2 ± 1.1

* Raw age. ** Ages are corrected for detrital derived ²³⁰Th using a ²³²Th/²³⁸U weight ratio of 3.8 ± 1.9 and ²³⁰Th, ²³⁴U, and ²³⁸U in secular equilibrium. Errors are 2σ. IUP-5550, IUP-5551, and IUP-5552 were analyzed by TIMS, and all other samples by MC-ICPMS. Dft: distance from top; AR: activity ratio.

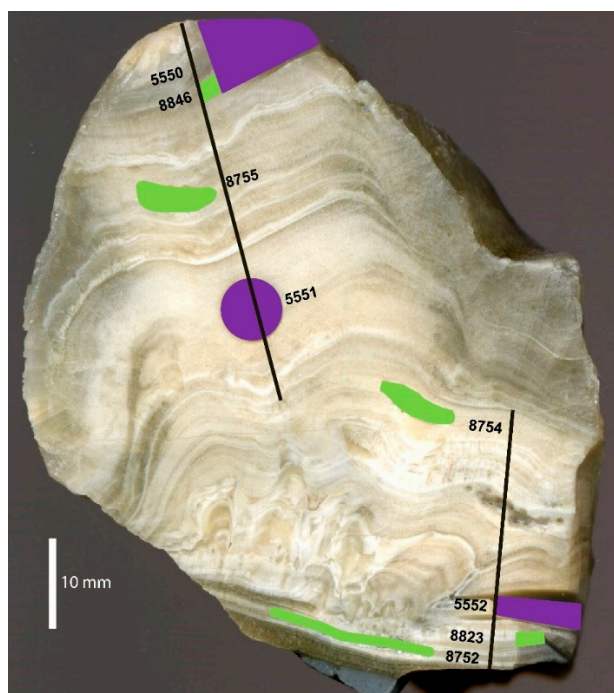


Figure 2. Cross-section of speleothem Kf-21. Positions for TIMS dates are marked with purple polygons; MC-ICPMS dates are marked with green polygons. ID-numbers correspond to ID-numbers in Table 1. Note the large samples for TIMS dating. The position of the sampling for carbon and oxygen isotope compositions is indicated by black lines.

The methods of sample preparation and mass spectrometric analysis follow the procedure of Ref. [2,38–42]. Activity ratios were analyzed with a Thermo Fisher Neptune MC-ICPMS and a TIMS MAT 262 at the Institute of Environmental Physics, University of Heidelberg, Germany. The calibration of the used ^{233}U , ^{236}U , and ^{229}Th spikes is described in Ref. [43]. For the MC-ICPMS analyses, replicated measurements of the HU-1 standard yielded activity ratios of ($^{234}\text{U}/^{238}\text{U}$) at 1.00002 ± 0.00082 and for ($^{230}\text{Th}/^{238}\text{U}$) at 1.0004 ± 0.0018 (errors given as 1σ of 517 measurements spanning 22 months) [42]. Blanks are smaller than 0.4 fg for ^{234}U and 0.04 fg for ^{230}Th . Ages were calculated using the half-lives from Cheng et al. [44]. Correction for detrital contamination assumes a $^{232}\text{Th}/^{238}\text{U}$ weight ratio of 3.8 ± 1.9 and ^{230}Th , ^{234}U , and ^{238}U in secular equilibrium. Age uncertainties are quoted at the 2σ -level and do not include half-life uncertainties.

For carbon and oxygen isotope composition analyses, sub-samples ($\sim 250 \mu\text{g}$) were drilled using a hand drill at 1 mm resolution. The subsampling was performed along an inferred growth axis subdivided into two tracks (Figure 2). In the lower section of the specimen, subsampling was conducted in the area with the least complex patterns in the calcite matrix (Figure 2, the lower black line).

Sub-samples were analyzed using an Isotopic Ratio Mass Spectrometer (IRMS) at the Department of Geological Sciences, Stockholm University. 100 microliters of 99% H_3PO_4 was added to each sample for reacting to carbon dioxide, and sub-samples were flushed with helium gas in septum-seal glass vials. For the analyses of stable isotope signatures, a GasbenchII device coupled to a Thermo Scientific MAT 253 mass spectrometer was used. Carbon and oxygen isotope compositions are reported as $\delta^{13}\text{C}$ and $\delta^{18}\text{O}$ in ‰ (per mil) relative to Vienna Pee Dee Belemnite (V-PDB). Based on repeated measurements of NBS19 and NBS18 standard materials, the reproducibility was calculated to be better than 0.07‰ for $\delta^{13}\text{C}$ and 0.15‰ for $\delta^{18}\text{O}$.

4. Results

4.1. Chronology

The results from the U-series analysis reveal uranium concentrations ranging between 492 to 1976 ng/g, which is sufficiently high for retrieving accurate dates with errors smaller than ~1 ka (MC-ICPMS) (Table 1). The detrital contamination, as indicated by the ^{232}Th concentrations, is moderate for all sub-samples, leading to age corrections of 100 to 800 years (with the exception of sample 8823, which gets a correction of 1.66 ka).

Age-depth modeling was performed by applying a Bayesian statistical approach using the StalAge algorithm (v. 1.0) [45] in combination with linear interpolation. Only MC-ICPMS ages were included in the age-depth modeling. In StalAge, the bottom-most U-Th age 130.17 ± 0.66 ka (ID 8752) was omitted because of the inability of the algorithm to account for the rapid change in growth rate. Instead, the bottom-most U-Th age was used to create a linear age-depth model from the oldest age modeled by StalAge (Figure 3).

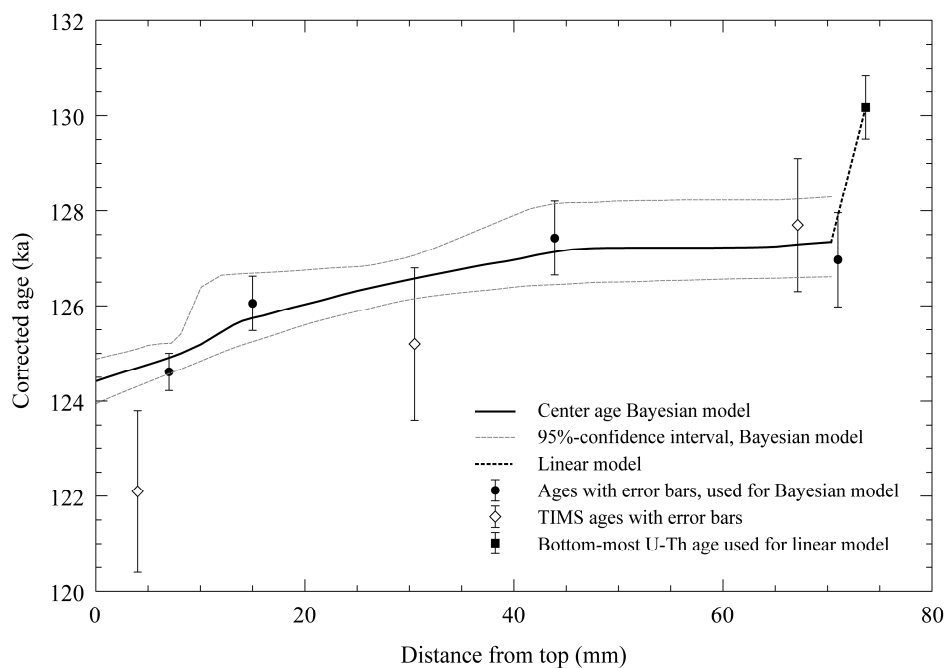


Figure 3. Bayesian age-depth model with 95% confidence interval for Kf-21 based on MC-ICPMS ages. Linear age-depth model created for bottom most part shown by dashed line. TAMS ages provide support for the created age-depth but were not included due to large uncertainties. Please note that the amount of material sampled for TAMS ages was large (see Figure 2). All U-Th ages are shown with 2σ error bars.

The three TAMS dates offer some support for the described age-depth model based on the MC-ICPMS dates. Two out of the three TAMS dates fit within the confidence error of the established age-depth mode (Figure 3). The third TAMS date (the youngest) falls just outside (Figure 3). However, considering that the amount of sample material was considerably larger, both in vertical distance and depth (Figure 2) and thus further away from the central growth axis, slightly younger TAMS dates compared to the MC-ICPMS dates can be expected.

The age-depth model suggests that the growth rate of Kf-21 during the initial growth period (130.17 ± 0.66 ka to ~ 127.3 ka) was approximately 1.2 mm/ka. This interval was followed by a period with substantially faster growth from ~ 127.3 to 127.2 ka. The growth rate then stabilized at a mean rate of ~ 19 mm/ka, although continuously decreasing until Kf-21 stopped growing at 124.4 ± 0.47 ka.

4.2. The $\delta^{13}\text{C}$ and $\delta^{18}\text{O}$ Records

The temporal resolution at the beginning of the main growth period (~127.3–124.4 ka) is ~25 years and gradually decreases to ~90 years towards the end of the speleothem formation. In the initial growth period from 130.17 ± 0.66 ka to ~127.3 ka, constrained to the base of the speleothem, the temporal resolution is low, with only three $\delta^{13}\text{C}$ and $\delta^{18}\text{O}$ values covering this period, and it is unclear whether growth was continuous. $\delta^{13}\text{C}$ and $\delta^{18}\text{O}$ values along the growth axis range from -11.6 to -8.0 ‰ and from -9.8 to -8.6 ‰, respectively (Figure 4 and Supplementary Table S1). The $\delta^{18}\text{O}$ record starts at the base of the speleothem where the temporal resolution is low, with values around -9.1 ‰. The values range between -9.8 ‰ and -8.6 ‰ during the subsequent, faster growth period that started at 127.3 ka and ended at 124.4 ka. A brief period with more negative $\delta^{18}\text{O}$ values is centered at ~127.0 ka, and periods with relatively less negative $\delta^{18}\text{O}$ values are centered at 127.25 ka, 126.1 ka, and 125.7 ka, respectively. Compared to the $\delta^{18}\text{O}$ time series, the $\delta^{13}\text{C}$ record shows smaller short-term variations but a more pronounced trend from more negative values at the beginning of the faster growth phase towards less negative values at the end of the growth period. After an initial decrease from -10.0 to -11.0 ‰ during the slow growth period, there is a sharp peak, centered at 127.25 ka, with values of up to -9.2 ‰, coinciding with the peak in $\delta^{18}\text{O}$. Thereafter (~127.2–126.9 ka), values decrease to -11.6 ‰ before they gradually increase to -8.3 ‰ at 124.4 ka.

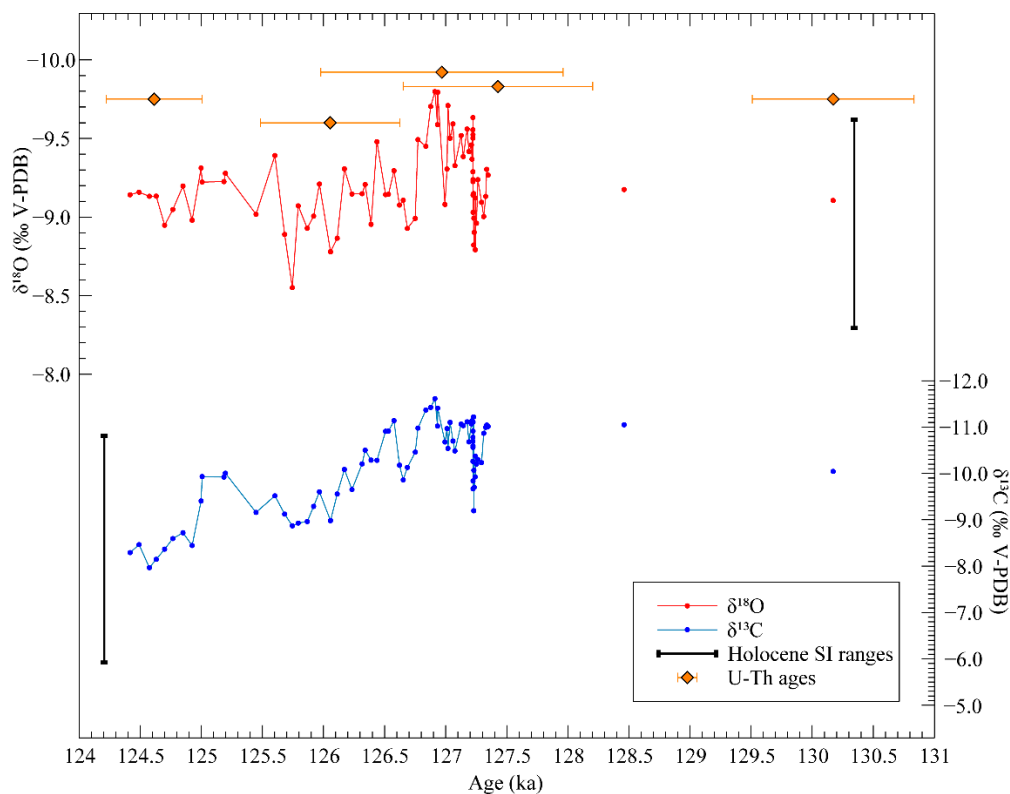


Figure 4. $\delta^{13}\text{C}$ and $\delta^{18}\text{O}$ from Kf-21 together with U-Th ages with error bars. Black vertical bars show the range of $\delta^{13}\text{C}$ and $\delta^{18}\text{O}$ in early- to mid-Holocene stalagmite K1 from Korallgrottan [14].

There is a positive correlation between $\delta^{13}\text{C}$ and $\delta^{18}\text{O}$ along the growth axis ($r = 0.63$; $n = 79$; $P < 0.001$). There is no distinct shift in isotope values between the upper and lower parts of the speleothem, and overlapping samples from the respective areas yielded similar results.

5. Discussion

5.1. Interpretation of Carbon and Oxygen Isotope Compositions

Modern monitoring of the cave atmosphere suggests that stable isotope compositions are likely not influenced by kinetic fractionation due to low temperatures and high relative humidity leading to a slow growth rate of speleothems in the cave [14,46,47]. A Hendy Test [48] was not performed because of the discussions around the validity of this test to investigate isotopic equilibrium conditions [49]. The positive relationship between $\delta^{13}\text{C}$ and $\delta^{18}\text{O}$ along the growth axis in Kf-21 is likely the result of climate and environmental factors that influence both isotopes.

The interpretation of carbon and oxygen isotope compositions in this paper follows previous interpretations from Korallgrottan based on modern monitoring and analyses of Holocene stalagmites [14,46]. Oxygen isotope compositions in speleothems can, under favorable conditions, reflect the $\delta^{18}\text{O}$ of the parent drip water (e.g., [50,51]). Drip water $\delta^{18}\text{O}$ is controlled by precipitation $\delta^{18}\text{O}$, processes that occur during transport through the epikarst, and the bedrock above the cave (e.g., [52,53]). Previous studies in Korallgrottan and caves in Norway have found a negative relationship between speleothem $\delta^{18}\text{O}$ and temperatures [14,18,46,54,55] following the negative relationship between water-calcite fractionation [56,57]. The present day climate above Korallgrottan is pronouncedly seasonal, and the isotopic composition of precipitation has been shown to be $\sim 5\text{‰}$ lighter (more negative) in winter compared to summer [14]. The observed negative relationship between speleothem $\delta^{18}\text{O}$ and temperature during interglacial conditions can be explained by variable ratios of isotopically heavier (less negative) summer precipitation and lighter (more negative) winter precipitation, as explained below. At present (interglacial) conditions, when the ground is frozen for five to six months, winter precipitation and spring meltwater must drain as surface runoff [14]. In the case of Korallgrottan, it has been suggested that during colder periods within an interglacial, the contribution of winter precipitation to drip water is further restricted because the ground is frozen for a longer period. The decrease in relative contribution of winter precipitation to the drip water therefore leads to less negative $\delta^{18}\text{O}$ values when the climate is colder, amplifying any effect of the water-calcite fractionation relationship [46]. Conversely, during periods of a warmer climate within an interglacial, a larger proportion of winter precipitation will infiltrate the bedrock and form drip water, leading to more negative $\delta^{18}\text{O}$ values in this water and ultimately in speleothems forming in the cave. In short, more negative $\delta^{18}\text{O}$ values in cave sinters are interpreted to reflect warmer conditions and less negative $\delta^{18}\text{O}$ values to reflect colder conditions.

Speleothem $\delta^{13}\text{C}$ remains more complex to interpret than $\delta^{18}\text{O}$. Carbon isotope compositions in speleothems have often been linked to biological activity, including microbial activity, in the soil above the cave, but other factors such as prior calcite precipitation, carbon component from the host rock, atmospheric CO_2 , and the CO_2 of the soil zone, as well as CO_2 resulting from decay of organic material found within the vadose zone, affect speleothem $\delta^{13}\text{C}$ values [52,58]. Previous work in Korallgrottan has suggested a link between vegetation density, controlled by temperature and humidity, and $\delta^{13}\text{C}$ values, but no firm links have been established [14,46]. Therefore, we only tentatively link $\delta^{13}\text{C}$ values to vegetation density during the LIG but do not provide a detailed interpretation of the $\delta^{13}\text{C}$ signal.

5.2. Climate Interpretation and Comparison with Scandinavian Speleothem Records

Following the age-depth model, Kf-21 formed during a period extending from 130.17 ± 0.66 ka to 124.4 ± 0.47 ka (Figure 3). Few isotope samples cover the slow-growing bottom-most (oldest) part of Kf-21, from 130.17 ± 0.66 ka to ~ 127.3 ka, so detailed climatic or environmental information from that period is not available. However, the fact that stalagmite Kf-21 grew in Korallgrottan during that time interval provides important information about the environmental setting and, in turn, the climate of the area in the early stages of the LIG. Since speleothem growth in this region only can occur when there is no ice sheet or permafrost [17,55], the formation of Kf-21 indicates that the area above Korallgrottan was neither under an ice sheet nor affected by permafrost from 130.17 ± 0.66 ka. Additionally, it can be

inferred that there was dripping water in the cave at least during parts of the year and that the cave was not ice filled year around. The area above the cave likely had a soil cover sustaining biological activity, likely a vegetation cover that was sufficient to produce enough CO₂ to acidify soil water sufficiently to cause chemical weathering of the bedrock. However, Atkinson [59] found actively growing speleothems in a cave under an ice field in Canada and attributed this to non-biogenic mechanisms including the oxidation of pyrite to sulfuric acid. Similarly, Spötl et al. [60] described actively forming speleothems under warm-based glaciers in the European Alps during the last glacial period (MIS 3). This formation process was independent of a source for pedogenic carbon dioxide and could operate when no soil and vegetation were present in these high elevation environments. Under such environmental conditions, however, speleothem $\delta^{13}\text{C}$ values are high and primarily reflect those of the host rock, which is the only source of carbon [60]. Considering that Korallgrottan is formed in calcite limestone or marble with little or no dolomite, gypsum, or pyrite present, and the relatively low $\delta^{13}\text{C}$ values that are within the range of Holocene values from speleothems that formed when soil and vegetation clearly were developed above Korallgrottan (Figure 4; [46]), the processes described by Atkinson [59] and Spötl et al. [60] do not seem likely.

From ~127.23 ka, the $\delta^{18}\text{O}$ values rapidly shift towards more negative values, and relatively stable $\delta^{18}\text{O}$ values are maintained until ~127.02 ka when there is a short-lived return to less negative values. While $\delta^{18}\text{O}$ shifts by 0.6‰, there is seemingly no change in $\delta^{13}\text{C}$ values at this time in Kf-21. From ~126.93 ka until ~126.77 ka, more negative $\delta^{18}\text{O}$ values are evident again, similar to the level before the event-like shift at ~127.02 ka. Interpreting the $\delta^{18}\text{O}$ variations as explained and motivated above, less negative $\delta^{18}\text{O}$ values are indicative of colder temperature conditions above the cave, whereas more negative values are indicative of warmer climate conditions. All comparisons with other archives mentioned in the text and figures below are based on that interpretation, and the axes have therefore been plotted accordingly. The period of overall warmer conditions between ~127.23 and ~126.77 ka also corresponds to the period of the most negative $\delta^{13}\text{C}$ values that may be linked to increased biological activity under warmer climate conditions. A stalagmite (FM-2) from Okshola, Norway, located approximately 270 km north of Korallgrottan, close to the Atlantic coast at 160 m a.s.l., started forming at 145 ± 5 ka [17]. The growth of this stalagmite was very slow (1–4 mm/10 ka) until 128 ± 5 ka when there was an increase in the growth rate. Oxygen isotope compositions from Okshola indicate a period of warmer temperatures from 128 ± 5 ka until 115 ± 5 ka [17]. The earlier onset of growth in Okshola needs to be viewed with the uncertain dating of this record in mind. At 145 ka, i.e., during Marine Isotope Stage 6, Scandinavia and the adjacent shelf areas were entirely covered by the ice of the Fennoscandia Ice Sheet [61], and it seems improbable that growth commenced this early at Okshola. Although one needs to account for the larger uncertainties of the Okshola record, there is a similar timing of the shift to warmer temperatures indicated by the $\delta^{18}\text{O}$ in FM-2 and Kf-21 at ~127.23 ka.

The termination of growth in Kf-21 cannot securely be linked to climatological factors. There is no evidence from growth rate or carbon and oxygen isotope compositions that there was a gradual or abrupt shift towards colder and/or drier conditions that ended growth. In fact, rapid growth in a stalagmite from Hamarnes Cave (~220 m a.s.l.), Norway, located ~165 km to the north of Korallgrottan suggests favorable growth conditions between ~123.35 and ~119.5 ka [18]. Similarly, the record from Okshola suggests that warm conditions continued until ~115 ka [17]. Both of these records further suggest that the growth termination in Kf-21 is not linked to climate. Instead, potential scenarios could include that the original drip position shifted or clogged, or that the large flowstone in Korallgrottan dislodged from its original growth position, which meant that growth could not continue. The lack of data after 124.4 ± 0.47 ka from Korallgrottan means there is no overlap with the record from Hamarnes Cave, and it prevents long-term comparisons with the Okshola record and an understanding of how the $\delta^{18}\text{O}$ values from Kf-21 changed during the full sequence of the LIG from deglaciation to the intensification of the glaciation that followed.

5.3. Comparison with Speleothem Records from Other Parts of Europe

A number of speleothem records from central Europe and the Mediterranean that cover parts of, or the full, LIG have been published over the years [2,31–35,37,62–71]. Here, we utilize some of these records to compare and put the carbon and oxygen isotope compositions and growth rate information from Korallgrottan in a broader paleoclimatic context. The focus of our comparison is on (1) the timing of the commencement of growth at ~130 ka; (2) the time around 127.3 ka when growth rate increased along with rapidly shifting but overall negative $\delta^{18}\text{O}$ values; and (3) the period of relatively less negative $\delta^{18}\text{O}$ values between ~126.77 and ~125.68 ka, in Kf-21.

In Schneckloch Cave and Hölloch Cave, located at ~1300 m a.s.l. in the Austrian Alps (Figure 1), ice-free, warmer, and wetter conditions are indicated from 134.1 ± 0.7 ka by the deposition of speleothems [32]. A rapid change towards less negative $\delta^{18}\text{O}$ values in stalagmites from these caves at 130.9 ± 0.9 ka (Figure 5C,D) suggests rapidly increasing temperatures in the region and a northward displacement of the polar front [32]. The timing of this shift is in good agreement with the onset of the deposition of Kf-21. There are also several other similarities between the $\delta^{18}\text{O}$ records from Schneckloch Cave and from Korallgrottan; for instance, there is a good agreement between warmer conditions interpreted from the less negative $\delta^{18}\text{O}$ values observed in Schneckloch Cave from ~127.1 to ~126.8 ka and more negative $\delta^{18}\text{O}$ values in Korallgrottan from ~127.23 to ~126.77 ka. These intervals are then followed by colder conditions in both caves indicated by more negative $\delta^{18}\text{O}$ values between ~126.8 and ~125.6 ka in Schneckloch Cave and less negative $\delta^{18}\text{O}$ values between ~126.77 and ~125.68 ka in Korallgrottan (Figure 5). To the east, growth of stalagmite BAR-II from Baradla Cave in northeast Hungary suggests that temperature and humidity conditions were suitable for speleothem formation from ~129 ka [31]. Carbon isotope compositions in stalagmite BAR-II show that interglacial conditions gradually developed from ~128 ka (Figure 5B), and that the period from ~127 to ~123 ka was one of higher humidity before full interglacial conditions were reached at ~124 ka [31]. The onset of the period of higher humidity in Baradla fits well with the start of more rapid growth and warmer conditions recorded in northwest Sweden. In Baradla Cave, a period of more negative $\delta^{13}\text{C}$ values in the interval of 126.8 to 125.7 ka coincides with the less negative $\delta^{18}\text{O}$ values in Korallgrottan between ~126.77 and ~125.68 ka. To the west, the formation of stalagmite BD-inf between ~128 and ~121 ka in Bourgeois-Delaunay Cave (western France) coincides with the warmest part of the LIG, and the most negative $\delta^{18}\text{O}$ values occur at ~127.7 ka (Figure 5E, [33]). The high-resolution $\delta^{18}\text{O}$ record from this cave suggests millennial-scale climate variability during the period from ~128 to ~121 ka, with several periods of drier conditions indicated by less negative $\delta^{18}\text{O}$ values, interrupting the overall wetter and warmer climate. One of the drier periods occurs between ~126.3 and ~125.3 ka, closely coinciding with the interval of colder climate conditions recorded in Korallgrottan between ~126.77 and ~125.68 ka (Figure 5A,E).

A new, high-resolution stacked $\delta^{18}\text{O}$ record based on data from several stalagmites from Corchia Cave, central Italy, shows persistent millennial-scale climate variability during the LIG that is linked to cold water events in the North Atlantic [36]. This new record is anchored by 87 U-Th ages from different stalagmites that provides a refined chronology for data from this cave published previously (e.g., [34–36]). An amelioration of climate conditions indicated by a shift to more negative $\delta^{18}\text{O}$ values occurs around 132 ± 1.3 ka [36]. Full interglacial conditions, i.e., warm and humid, are suggested by most negative $\delta^{18}\text{O}$ values between ca. ~129.3 and ~127 ka. A distinct interval with less negative $\delta^{18}\text{O}$ values, indicating increased aridity, is recorded in the time interval of $127\text{--}126 \pm 0.7$ ka in Corchia, which is in close concordance with the cold conditions recorded in Korallgrottan between ~126.77 and ~125.68 ka (Figure 5F). Reduced precipitation over Corchia Cave can be linked to colder surface waters in the North Atlantic that leads to reduced evaporation [35,36]. The dry interval between ~127 and ~126 ka in Corchia, suggested to be associated with reduced Atlantic meridional overturning circulation (AMOC) and cold sea surface temperatures (SST) in the North Atlantic, is further supported by climate modeling experiments [36]. A $\delta^{18}\text{O}$ record from Tana che Urla Cave, located close to Corchia Cave, shows peak interglacial conditions between ~131.0 and ~123.6 ka (Figure 5G; [37]). Most negative $\delta^{18}\text{O}$ values were reached in Tana che Urla at $128\text{--}128.5 \pm 0.9$ ka and a brief period of less negative $\delta^{18}\text{O}$ values indicating drier conditions is recorded between ~126.7 and ~125.6 ka

(Figure 5G; [37]). Regattieri et al. [37] linked this dry interval to a southward displacement of the polar front, enhancing cyclogenesis in the sub-polar North Atlantic and moisture transport to northern and western Europe, meaning that less precipitation reached the cave sites further south.

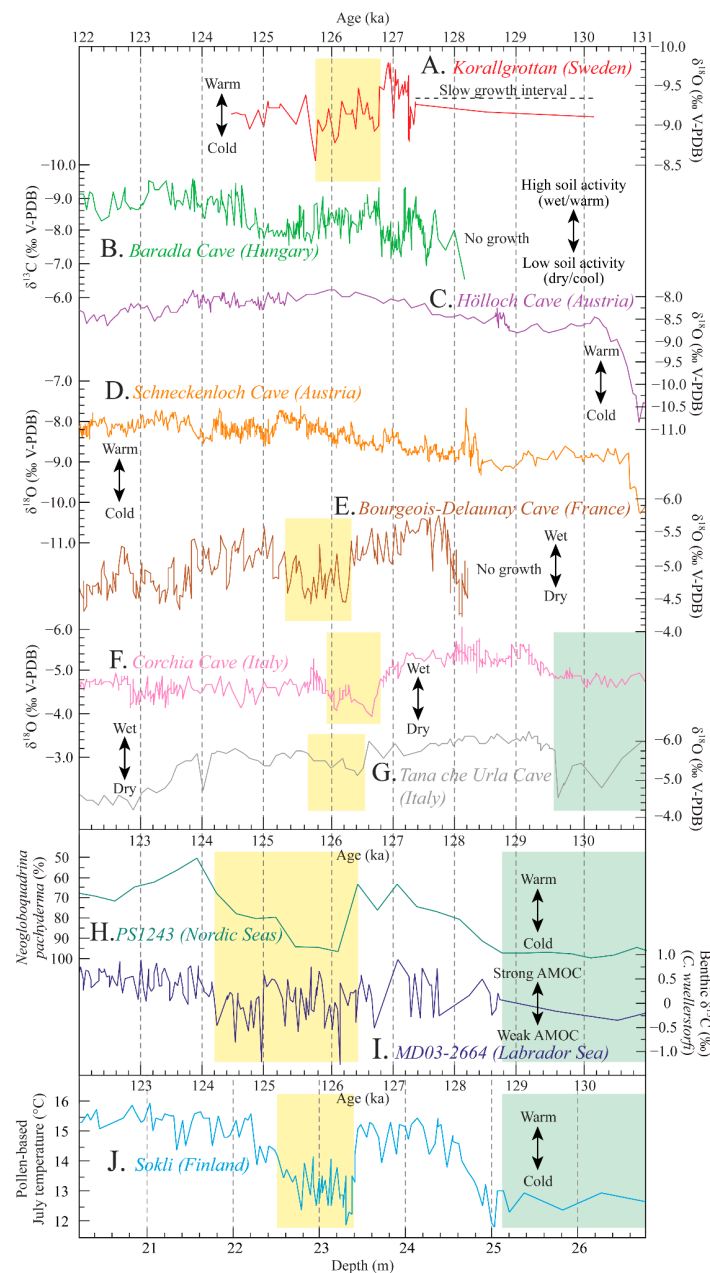


Figure 5. Comparison between $\delta^{18}\text{O}$ in Kf-21 and other speleothem records from other parts of Europe arranged from north to south (upper part) and between $\delta^{18}\text{O}$ in Kf-21 and reconstructed summer temperatures from Sokli (northeast Finland) and sites in the North Atlantic (lower part). A: Korallgrottan, Kf-21, this study; B: Baradla Cave, $\delta^{13}\text{C}$ from stalagmite BAR-II #B [31]; C: Hölloch, $\delta^{18}\text{O}$ from stalagmite HÖL-10 [32]; D: Schneckloch, $\delta^{18}\text{O}$ from stalagmite SCH-5 [32]; E: Bourgeois-Delaunay Cave, $\delta^{18}\text{O}$ in stalagmite BD-inf [33]; F: Corchia Cave, stacked $\delta^{18}\text{O}$ [36]; G: Tana che Urla, $\delta^{18}\text{O}$ from stalagmite D4 [37]; H and I: North Atlantic sites PS1243 [27,28] and MD03-2664 [30]; J: Sokli T_{Jul} [22]. For location of sites, see Figure 1. Yellow bars indicate the cold period in Korallgrottan between ~ 126.77 and ~ 125.68 ka that is nearly coeval with drier conditions in three other caves sites and evidence for weak Atlantic meridional overturning circulation (AMOC) and low temperatures in the North Atlantic as well as in Sokli (northeast Finland). Green bar indicates early LIG cold conditions.

What is clear from the above comparisons is that there are similarities in the timing between the start of growth in Kf-21, as well as the increase in growth rate paired with isotopic indications of a warmer climate in high latitude Europe at ~127.3 ka, and indications of wetter and warmer climate conditions in other parts of Europe, and the Mediterranean. Govin et al. [10] reports that around 128–127 ka, there is a relatively synchronous change towards higher growth rates in speleothems from Europe, but that growth inception is delayed in the north compared to the south. They suggest that the onset of growth may be linked to temperature thresholds that need to be reached before speleothem formation starts. However, the results from Kf-21, together with the stalagmite from Okshola [17], suggest that the onset of growth during the LIG may have been earlier than previously suggested along the Atlantic seaboard in northern Europe. Initiation of growth was, however, still delayed in comparison with records from southern Europe and the Mediterranean, likely because of the time it took to melt the Fennoscandian Ice Sheet. It can be noted that the area above Korallgrottan was one of the last areas to be deglaciated following the last glaciation [72].

5.4. Comparisons with Other Nearby Terrestrial and Marine Climate Archives

Sediments in northern Europe dated to the LIG are rare due to a highly fragmented sediment record resulting from glacial erosion and poor dating control. However, a thick lake deposit of Eemian age (bracketed by thermoluminescence and infrared stimulated luminescence dating to >~110 and <~150–180 ka, and OSL dating on quartz to >~95 ka), and found in sequence with overlying glacial and non-glacial sediments of Weichselian age, is preserved in the Sokli basin in northeast Finland [11,29,73,74]. The analysis of multiple paleo-environmental and climatic proxies from the 12-m-thick deposit has resulted in a unique high-resolution record for the LIG from a similar high-latitude European site as Korallgrottan in northwest Sweden [19–22]. Pollen-based reconstructions show an early onset of interglacial conditions with the establishment of boreal forest and mean July air temperatures reaching ~2 °C higher than today. The warm summers are supported by diatom and geochemical data recording stable lake stratification. Warming was suddenly halted by the so-called Tunturi cooling event where a drop in July temperatures of ca. 2–4 °C caused the boreal forest to be replaced by open birch-pine forest [19,22]. The multi-proxy evidence indicates that the cooling was accompanied by drying, causing drops in lake level. More favorable climate conditions were achieved directly following the Tunturi event; the pollen-based temperature reconstruction shows July temperatures to surpass current values by 2–3 °C. The multiproxy evidence from Sokli also suggests a distinct shift in continentality over the LIG. Evidence from Sokli suggests continental conditions for the early LIG [20], which might explain the slow growth rates at the start of the Kf-21 speleothem record. In the late LIG, Sokli underwent a shift towards a more oceanic climate, with pollen-based reconstructions indicating a rise in mean January temperature [22], supported by diatom evidence for mild winters [20].

The Kf-21 $\delta^{18}\text{O}$ record and the pollen-based July temperature at Sokli thus show a similar sequence of events for the early LIG, including a short-lived warm phase followed by an abrupt cooling. We thus suggest the onset of cooling at Korallgrottan at 126.77 ka (Figure 5) might correspond with the onset of the cold and dry Tunturi Event at Sokli (Figure 5) [19,22]. While the cooling at Sokli occurs approximately 1.5 ka earlier, the Sokli series has only a tentative absolute chronology based on aligning the onset and end of interglacial conditions (indicated by the pollen data) with Austrian and Belgian stalagmite data [22]. Based on the available absolute chronologies and the sequence of events across the LIG, Salonen et al. [22] tie the Tunturi event with disturbances in the North Atlantic oceanic circulation regime, visible in proxies for both AMOC strength (Figure 5I; [30]) and SST's in the central Nordic Seas (Figure 5H; [27,28]). Tzedakis et al. [36] later tied the same marine events with an abrupt onset of drought in southern Europe, indicated by an increase in $\delta^{18}\text{O}$ at Corchia cave (Figure 5F) and a drop in pollen from temperate trees in a marine core at the Portuguese margin. Based on sediments from the North Atlantic, Mokeddem et al. [75] suggested that short-term, millennial, southward displacements of the polar front during the LIG lead to an extension on cold sea surface water and sea ice in the

North Atlantic. The onset of cold conditions at Korallgrottan at ~126.77 ka matches closely (well within dating uncertainties) with both the drop in sea surface temperatures and AMOC events as well as with the onset of drought in southern Europe (Figure 5). Based on the coherent timing of the downturn in temperature and precipitation proxies, including robustly dated speleothems from northwest Sweden, west France and central Italy, we suggest that an abrupt climate event driven by a disturbance of North Atlantic circulation interrupted the LIG in Europe, with a climatic signal spanning from the Mediterranean to the Arctic.

6. Conclusions

The new Kf-21 record from Korallgrottan, northwest Sweden, reveals that relatively warm climate conditions above the cave, allowing for the accumulation of soil, and vegetation growth prevailed already at around 130 ka, providing the first minimum absolute age determination for the timing of deglaciation of the central area of the Fennoscandian Ice Sheet following the penultimate glaciation (MIS 6). It suggests that speleothem formation in northernmost Europe commenced well before 128–127 ka as suggested by Govin et al. [10].

Following a period of slow growth rates possibly due to low precipitation (more continental climate regime) and low temperatures, a rapid increase in growth rate at ~127.3 ka and a shift to more negative $\delta^{18}\text{O}$ values in Kf-21 suggest overall warmer conditions in the area between ~127.23 and ~126.77 ka. This is similar to many other speleothem records from other parts of Europe and the Mediterranean.

Our record provides an insight to millennial-scale climate variability during the first half of the LIG from the high latitudes. Evidence of millennial-scale cooling between ~126.77 and ~125.68 ka above Korallgrottan occurs nearly concomitantly with drier conditions recorded in speleothems from central Italy and western France. This period can also be linked to cooler conditions recorded in lake sediments in Sokli, northeast Finland, colder SSTs in the North Atlantic, and a reduced AMOC. A reduced transport of heat and moisture to higher latitudes within this interval, resulting in a similar spatial climate pattern, has also been suggested by Demeny et al. [31], and our findings extends this picture further north than was previously possible. The co-occurrence of drier and colder conditions indicates climate instability across Europe in an interval centered around 126 ka.

Supplementary Materials: The following are available online at <http://www.mdpi.com/2571-550X/2/3/29/s1>, Table S1: Carbon and oxygen isotope compositions for Kf-21.

Author Contributions: Conceptualization, M.F., S.H., and K.F.H.; methodology, M.F., S.H., N.F., and A.S.-R.; software, M.F.; validation, M.F., S.H., S.S., K.F.H., M.D., N.F., and A.S.-R.; investigation, M.F., S.H., N.F., and A.S.-R.; resources, N.F. and A.S.-R.; writing—original draft preparation, M.F., S.H., S.S., and K.F.H.; writing—review and editing, A.S.-R. and M.D.; visualization, M.F. and S.S.; project administration, M.F. and S.H.; funding acquisition, K.F.H. and S.H.

Funding: This research received no external funding.

Acknowledgments: We thank Hanna Sundqvist for collecting and sharing the speleothem from Korallgrottan and for invaluable help with the interpretation of our results. We thank René Eichstädter at the Institute of Environmental Physics (Heidelberg University) for conducting the MC ICP-MS measurements and Heike Siegmund at the Department of Geological Sciences (Stockholm University) for the stable isotope analyses. We would also like to express our gratitude to the two anonymous reviewers whose comments improved the quality of the manuscript. Funding for stable isotope analyses was provided by the Bolin Centre for Climate Research at Stockholm University (Sweden). Karin F. Helmens further acknowledges funding from the Swedish Nuclear Fuel and Waste Management Company (SKB). Sakari Salonen was funded by the Academy of Finland (project 1310649).

Conflicts of Interest: The authors declare no conflict of interest

References

1. Henderson, G.M.; Slowey, N.C. Evidence from U–Th dating against Northern Hemisphere forcing of the penultimate deglaciation. *Nature* **2000**, *404*, 61–66. [[CrossRef](#)] [[PubMed](#)]

2. Holzkämper, S.; Spötl, C.; Mangini, A. High-precision constraints on timing of Alpine warm periods during the middle to late Pleistocene using speleothem growth periods. *Earth Planet. Sci. Lett.* **2005**, *236*, 751–764. [[CrossRef](#)]
3. Imbrie, J.; Hays, J.D.; McIntyre, A.; Mix, A.C.; Morley, J.J.; Pisias, N.G.; Prell, W.L.; Shackleton, N.J. The Orbital Theory of Pleistocene Climate: Support from a Revised Chronology of the Marine $\delta^{18}\text{O}$ Record. In *Milankovitch and Climate: Understanding the Response to Astronomical Forcing*; Berger, A., Imbrie, J., Hays, J., Kukla, G., Saltzman, B., Eds.; D. Reidel Publishing Company: Dordrecht, The Netherlands, 1984; pp. 269–305.
4. Bauch, H.A.; Kandiano, E.S.; Helmke, J.; Andersen, N.; Rosell-Mele, A.; Erlenkeuser, H. Climatic bisection of the last interglacial warm period in the Polar North Atlantic. *Quat. Sci. Rev.* **2011**, *30*, 1813–1818. [[CrossRef](#)]
5. Fronval, T.; Jansen, E. Rapid changes in ocean circulation and heat flux in the Nordic seas during the last interglacial period. *Nature* **1996**, *383*, 806–810. [[CrossRef](#)]
6. Sirocko, F.; Seelos, K.; Schaber, K.; Rein, B.; Dreher, F.; Diehl, M.; Lehne, R.; Jäger, K.; Krbetschek, M.; Degering, D. A late Eemian aridity pulse in central Europe during the last glacial inception. *Nature* **2005**, *436*, 833–836. [[CrossRef](#)] [[PubMed](#)]
7. Bakker, P.; Masson-Delmotte, V.; Martrat, B.; Charbit, S.; Renssen, H.; Gröger, M.; Krebs-Kanzow, U.; Lohmann, G.; Lunt, D.; Pfeiffer, M.; et al. Temperature trends during the Present and Last Interglacial periods – a multi-model-data comparison. *Quat. Sci. Rev.* **2014**, *99*, 224–243. [[CrossRef](#)]
8. Members, C.L. Last Interglacial Project Members Last Interglacial Arctic warmth confirms polar amplification of climate change. *Quat. Sci. Rev.* **2006**, *25*, 1383–1400.
9. Capron, E.; Govin, A.; Stone, E.J.; Masson-Delmotte, V.; Mulitza, S.; Otto-Bliesner, B.; Rasmussen, T.L.; Sime, L.C.; Waelbroeck, C.; Wolff, E.W. Temporal and spatial structure of multi-millennial temperature changes at high latitudes during the Last Interglacial. *Quat. Sci. Rev.* **2014**, *103*, 116–133. [[CrossRef](#)]
10. Govin, A.; Capron, E.; Tzedakis, P.; Verheyden, S.; Ghaleb, B.; Hillaire-Marcel, C.; St-Onge, G.; Stoner, J.; Bassinot, F.; Bazin, L.; et al. Sequence of events from the onset to the demise of the Last Interglacial: Evaluating strengths and limitations of chronologies used in climatic archives. *Quat. Sci. Rev.* **2015**, *129*, 1–36. [[CrossRef](#)]
11. Helmens, K.F. The Last Interglacial–Glacial cycle (MIS 5–2) re-examined based on long proxy records from central and northern Europe. *Quat. Sci. Rev.* **2014**, *86*, 115–143. [[CrossRef](#)]
12. Baker, A.; Ito, E.; Smart, P.L.; McEwan, R.F. Elevated and variable values of ^{13}C in speleothems in a British cave system. *Chem. Geol.* **1997**, *136*, 263–270. [[CrossRef](#)]
13. McDermott, F.; Matthey, D.P.; Hawkesworth, C. Centennial-scale Holocene climate variability revealed by a high-resolution speleothem $\delta^{18}\text{O}$ record from SW Ireland. *Science* **2001**, *294*, 1328–1331. [[CrossRef](#)] [[PubMed](#)]
14. Sundqvist, H.S.; Holmgren, K.; Lauritzen, S.E. Stable isotope variations in stalagmites from northwestern Sweden document climate and environmental changes during the early Holocene. *Holocene* **2007**, *17*, 259–267. [[CrossRef](#)]
15. Jiang, X.; Wang, X.; He, Y.; Hu, H.M.; Li, Z.; Spötl, C.; Shen, C.C. Precisely dated multidecadally resolved Asian summer monsoon dynamics 113.5–86.6 thousand years ago. *Quat. Sci. Rev.* **2016**, *143*, 1–12. [[CrossRef](#)]
16. Berstad, I.M.; Lundberg, J.; Lauritzen, S.E.; Linge, H.C. Comparison of the Climate during Marine Isotope Stage 9 and 11 Inferred from a Speleothem Isotope Record from Northern Norway. *Quat. Res.* **2002**, *58*, 361–371. [[CrossRef](#)]
17. Lauritzen, S.E. High-Resolution Paleotemperature Proxy Record for the Last Interglacial Based on Norwegian Speleothems. *Quat. Res.* **1995**, *43*, 133–146. [[CrossRef](#)]
18. Linge, H.; Lauritzen, S.E.; Lundberg, J. Stable Isotope Stratigraphy of a Late Last Interglacial Speleothem from Rana, Northern Norway. *Quat. Res.* **2001**, *56*, 155–164. [[CrossRef](#)]
19. Helmens, K.F.; Salonen, J.S.; Pliik, A.; Engels, S.; Väiliranta, M.; Kylander, M.; Brendryen, J.; Renssen, H. Major cooling intersecting peak Eemian Interglacial warmth in northern Europe. *Quat. Sci. Rev.* **2015**, *122*, 293–299. [[CrossRef](#)]
20. Pliik, A.; Helmens, K.F.; Fernández-Fernández, M.; Kylander, M.; Löwemark, L.; Risberg, J.; Salonen, J.S.; Väiliranta, M.; Weckström, J. Development of an Eemian (MIS 5e) Interglacial palaeolake at Sokli (N Finland) inferred using multiple proxies. *Palaeogeogr. Palaeoclimatol. Palaeoecol.* **2016**, *463*, 11–26. [[CrossRef](#)]
21. Pliik, A.; Engels, S.; Luoto, T.P.; Nazarova, L.; Salonen, J.S.; Helmens, K.F. Chironomid-based temperature reconstruction for the Eemian Interglacial (MIS 5e) at Sokli, northeast Finland. *J. Paleolimnol.* **2019**, *61*, 355–371. [[CrossRef](#)]

22. Salonen, J.S.; Helmens, K.F.; Brendryen, J.; Kuosmanen, N.; Väiliranta, M.; Goring, S.; Korpela, M.; Kylander, M.; Philip, A.; Pliikk, A.; et al. Abrupt high-latitude climate events and decoupled seasonal trends during the Eemian. *Nat. Commun.* **2018**, *9*, 2851. [[CrossRef](#)]
23. Isacsson, G. Vad kan man se i Korallgrottan? *Grottan* **1994**, *2*, 21–23.
24. Nilsson, G. *Berggrunden Inom Blåsjöområdet i Nordvästra Jämtlandsfjällen*; Sveriges Geologiska Undersökning Serie C 595: Stockholm, Sweden, 1964; p. 70.
25. Zackrisson, E.; Sjöstrand, T. *Berggrundskartorna 22D-22E Frostviken, 1:50 000*; SGU Ai 41-44: Uppsala, Sweden, 1990.
26. Alexandersson, H.; Eggertsson Karlström, C. *Temperaturen och Nederbörden i Sverige 1961–1990*; Referensnormaler—Utgåva 2; Meteorologi 99; Swedish Meteorological and Hydrological Institute: Norrköping, Sweden, 2001; p. 71.
27. Bauch, H.A.; Kandiano, E.S.; Helmke, J.P. Contrasting ocean changes between the subpolar and polar North Atlantic during the past 135 ka. *Geophys. Res. Lett.* **2012**, *39*, L11604. [[CrossRef](#)]
28. Zhuravleva, A.; Bauch, H.A.; Van Nieuwenhove, N. Last Interglacial (MIS5e) hydrographic shifts linked to meltwater discharges from the East Greenland margin. *Quat. Sci. Rev.* **2017**, *164*, 95–109. [[CrossRef](#)]
29. Helmens, K. The Last Interglacial-Glacial cycle in NE Fennoscandia: A nearly continuous record from Sokli (Finnish Lapland). *Quat. Sci. Rev.* **2000**, *19*, 1605–1623. [[CrossRef](#)]
30. Galaasen, E.V.; Ninnemann, U.S.; Irval, N.; Kleiven, H.F.; Rosenthal, Y.; Kissel, C.; Hodell, D.A.; Irvali, N. Rapid Reductions in North Atlantic Deep Water During the Peak of the Last Interglacial Period. *Science* **2014**, *343*, 1129–1132. [[CrossRef](#)] [[PubMed](#)]
31. Demény, A.; Kern, Z.; Czuppon, G.; Németh, A.; Leél-Őssy, S.; Siklósy, Z.; Lin, K.; Hu, H.M.; Shen, C.C.; Vennemann, T.W.; et al. Stable isotope compositions of speleothems from the last interglacial—Spatial patterns of climate fluctuations in Europe. *Quat. Sci. Rev.* **2017**, *161*, 68–80. [[CrossRef](#)]
32. Moseley, G.E.; Spötl, C.; Cheng, H.; Boch, R.; Min, A.; Edwards, R.L. Termination-II interstadial/stadial climate change recorded in two stalagmites from the north European Alps. *Quat. Sci. Rev.* **2015**, *127*, 229–239. [[CrossRef](#)]
33. Couchoud, I.; Genty, D.; Hoffmann, D.; Drysdale, R.; Blamart, D. Millennial-scale climate variability during the Last Interglacial recorded in a speleothem from south-western France. *Quat. Sci. Rev.* **2009**, *28*, 3263–3274. [[CrossRef](#)]
34. Drysdale, R.N.; Zanchetta, G.; Hellstrom, J.C.; Fallick, A.E.; Zhao, J.X. Stalagmite evidence for the onset of the Last Interglacial in southern Europe at 129 ± 1 ka. *Geophys. Res. Lett.* **2005**, *32*, L24708. [[CrossRef](#)]
35. Drysdale, R.N.; Hellstrom, J.C.; Zanchetta, G.; Fallick, A.E.; Goni, M.F.S.; Couchoud, I.; McDonald, J.; Maas, R.; Lohmann, G.; Isola, I.; et al. Evidence for Obliquity Forcing of Glacial Termination II. *Science* **2009**, *325*, 1527–1531. [[CrossRef](#)] [[PubMed](#)]
36. Tzedakis, P.C.; Drysdale, R.N.; Margari, V.; Skinner, L.C.; Menviel, L.; Rhodes, R.H.; Taschetto, A.S.; Hodell, D.A.; Crowhurst, S.J.; Hellstrom, J.C.; et al. Enhanced climate instability in the North Atlantic and southern Europe during the Last Interglacial. *Nat. Commun.* **2018**, *9*, 4235. [[CrossRef](#)] [[PubMed](#)]
37. Regattieri, E.; Zanchetta, G.; Drysdale, R.N.; Isola, I.; Hellstrom, J.C.; Roncioni, A. A continuous stable isotope record from the penultimate glacial maximum to the Last Interglacial (159–121 ka) from Tana Che Urla Cave (Apuan Alps, central Italy). *Quat. Res.* **2014**, *82*, 450–461. [[CrossRef](#)]
38. Arps, J. Towards ϵ -Precision of U-series Age Determinations of Secondary Carbonates. Ph.D. Thesis, Heidelberg University Library, Heidelberg, Germany, 2017.
39. Douville, E.; Sallé, E.; Frank, N.; Eisele, M.; Pons-Branchu, E.; Ayrault, S. Rapid and accurate U–Th dating of ancient carbonates using inductively coupled plasma-quadrupole mass spectrometry. *Chem. Geol.* **2010**, *272*, 1–11. [[CrossRef](#)]
40. Frank, N.; Braum, M.; Hambach, U.; Mangini, A.; Wagner, G. Warm Period Growth of Travertine during the Last Interglaciation in Southern Germany. *Quat. Res.* **2000**, *54*, 38–48. [[CrossRef](#)]
41. Matos, L.; Mienis, F.; Wienberg, C.; Frank, N.; Kwiatkowski, C.; Groeneveld, J.; Thil, F.; Abrantes, F.; Cunha, M.R.; Hebbeln, D. Interglacial occurrence of cold-water corals off Cape Lookout (NW Atlantic): First evidence of the Gulf Stream influence. *Deep. Sea Res. Part I Oceanogr. Res. Pap.* **2015**, *105*, 158–170. [[CrossRef](#)]
42. Wefing, A.M.; Arps, J.; Blaser, P.; Wienberg, C.; Hebbeln, D.; Frank, N. High precision U-series dating of scleractinian cold-water corals using an automated chromatographic U and Th extraction. *Chem. Geol.* **2017**, *475*, 140–148. [[CrossRef](#)]

43. Hoffmann, D.L.; Prytulak, J.; Richards, D.A.; Elliott, T.; Coath, C.D.; Smart, P.L.; Scholz, D. Procedures for accurate U and Th isotope measurements by high precision MC-ICPMS. *Int. J. Mass Spectrom.* **2007**, *264*, 97–109. [[CrossRef](#)]
44. Cheng, H.; Edwards, R.; Hoff, J.; Gallup, C.; Richards, D.; Asmerom, Y. The half-lives of uranium-234 and thorium-230. *Chem. Geol.* **2000**, *169*, 17–33. [[CrossRef](#)]
45. Scholz, D.; Hoffmann, D.L. StalAge—An algorithm designed for construction of speleothem age models. *Quat. Geochronol.* **2011**, *6*, 369–382. [[CrossRef](#)]
46. Sundqvist, H.S.; Holmgren, K.; Moberg, A.; Mangini, A.; Spöetl, C. Stable isotopes in a stalagmite from NW Sweden document environmental changes over the past 4000 years. *Boreas* **2010**, *39*, 77–86. [[CrossRef](#)]
47. Sundqvist, H.S.; Seibert, J.; Holmgren, K. Understanding conditions behind speleothem formation in Korallgrottan, northwestern Sweden. *J. Hydrol.* **2007**, *347*, 13–22. [[CrossRef](#)]
48. Hendy, C. The isotopic geochemistry of speleothems—I. The calculation of the effects of different modes of formation on the isotopic composition of speleothems and their applicability as palaeoclimatic indicators. *Geochim. Cosmochim. Acta* **1971**, *35*, 801–824. [[CrossRef](#)]
49. Dorale, J.A.; Liu, Z. Limitations of hendy test criteria in judging the paleoclimatic suitability of speleothems and the need for replication. *J. Cave Karst Stud.* **2009**, *71*, 73–80.
50. Lachniet, M.S. Climatic and environmental controls on speleothem oxygen-isotope values. *Quat. Sci. Rev.* **2009**, *28*, 412–432. [[CrossRef](#)]
51. McDermott, F. Palaeo-climate reconstruction from stable isotope variations in speleothems: A review. *Quat. Sci. Rev.* **2004**, *23*, 901–918. [[CrossRef](#)]
52. Fairchild, I.J.; Smith, C.L.; Baker, A.; Fuller, L.; Spötl, C.; Matthey, D.; McDermott, F. Modification and preservation of environmental signals in speleothems. *Earth Sci. Rev.* **2006**, *75*, 105–153. [[CrossRef](#)]
53. Fairchild, I.J.; Baker, A. *Speleothem Science: from Process to Past Environments*; Wiley: Hoboken, NJ, USA, 2012; ISBN 978-1-4051-9620-8.
54. Lauritzen, S.E.; Lundberg, J. Calibration of the speleothem delta function: An absolute temperature record for the Holocene in northern Norway. *Holocene* **1999**, *9*, 659–669. [[CrossRef](#)]
55. Linge, H.; Baker, A.; Andersson, C.; Lauritzen, S.E. Variability in luminescent lamination and initial ²³⁰Th/²³²Th activity ratios in a late Holocene stalagmite from northern Norway. *Quat. Geochronol.* **2009**, *4*, 181–192. [[CrossRef](#)]
56. Kim, S.T.; O'Neil, J.R. Equilibrium and nonequilibrium oxygen isotope effects in synthetic carbonates. *Geochim. Cosmochim. Acta* **1997**, *61*, 3461–3475. [[CrossRef](#)]
57. Tremaine, D.M.; Froelich, P.N.; Wang, Y. Speleothem calcite formed in situ: Modern calibration of $\delta^{18}\text{O}$ and $\delta^{13}\text{C}$ paleoclimate proxies in a continuously-monitored natural cave system. *Geochim. Cosmochim. Acta* **2011**, *75*, 4929–4950. [[CrossRef](#)]
58. Matthey, D.; Atkinson, T.; Barker, J.; Fisher, R.; Latin, J.P.; Durrell, R.; Ainsworth, M. Carbon dioxide, ground air and carbon cycling in Gibraltar karst. *Geochim. Cosmochim. Acta* **2016**, *184*, 88–113. [[CrossRef](#)]
59. Atkinson, T.C. Growth Mechanisms of Speleothems in Castleguard Cave, Columbia Icefields, Alberta, Canada. *Arct. Alp. Res.* **1983**, *15*, 523–526. [[CrossRef](#)]
60. Spötl, C.; Mangini, A.; Richards, D.A. Chronology and paleoenvironment of Marine Isotope Stage 3 from two high-elevation speleothems, Austrian Alps. *Quat. Sci. Rev.* **2006**, *25*, 1127–1136. [[CrossRef](#)]
61. Svendsen, J.L.; Alexanderson, H.; Astakhov, V.I.; Demidov, I.; Dowdeswell, J.A.; Funder, S.; Gataullin, V.; Henriksen, M.; Hjort, C.; Houmark-Nielsen, M.; et al. Late Quaternary ice sheet history of northern Eurasia. *Quat. Sci. Rev.* **2004**, *23*, 1229–1271. [[CrossRef](#)]
62. Badertscher, S.; Fleitmann, D.; Cheng, H.; Edwards, R.L.; Gökürk, O.M.; Zumbühl, A.; Leuenberger, M.C.; Tüysüz, O. Pleistocene water intrusions from the Mediterranean and Caspian seas into the Black Sea. *Nat. Geosci.* **2011**, *4*, 236–239. [[CrossRef](#)]
63. Bar-Matthews, M.; Ayalon, A.; Gilmour, M.; Matthews, A.; Hawkesworth, C.J. Sea–land oxygen isotopic relationships from planktonic foraminifera and speleothems in the Eastern Mediterranean region and their implication for paleorainfall during interglacial intervals. *Geochim. Cosmochim. Acta* **2003**, *67*, 3181–3199. [[CrossRef](#)]
64. Boch, R.; Cheng, H.; Spötl, C.; Edwards, R.L.; Wang, X.; Häuselmann, P. NALPS: A precisely dated European climate record 120–60 ka. *Clim. Past* **2011**, *7*, 1247–1259. [[CrossRef](#)]
65. Holzkämper, S.; Mangini, A.; Spötl, C.; Mudelsee, M. Timing and progression of the Last Interglacial derived from a high alpine stalagmite. *Geophys. Res. Lett.* **2004**, *31*, L07201. [[CrossRef](#)]

66. Meyer, M.C.; Spötl, C.; Mangini, A. The demise of the Last Interglacial recorded in isotopically dated speleothems from the Alps. *Quat. Sci. Rev.* **2008**, *27*, 476–496. [[CrossRef](#)]
67. Muñoz García, M.B.; Rossi, C.; Ford, D.C.; Schwarcz, H.P.; Martín Chivelet, J. Chronology of Termination II and the Last Interglacial Period in North Spain based on stable isotope records of stalagmites from Cueva del Cobre (Palencia). *J. Iber. Geol.* **2007**, *33*, 17.
68. Nehme, C.; Verheyden, S.; Noble, S.; Farrant, A.R.; Sahy, D.; Hellström, J.; Delannoy, J.J.; Claeys, P. Reconstruction of MIS 5 climate in the central Levant using a stalagmite from Kanaan Cave, Lebanon. *Clim. Past* **2015**, *11*, 1785–1799. [[CrossRef](#)]
69. Stoll, H.M.; Moreno, A.; Mendez-Vicente, A.; Gonzalez-Lemos, S.; Jimenez-Sanchez, M.; Dominguez-Cuesta, M.J.; Edwards, R.L.; Cheng, H.; Wang, X. Paleoclimate and growth rates of speleothems in the northwestern Iberian Peninsula over the last two glacial cycles. *Quat. Res.* **2013**, *80*, 284–290. [[CrossRef](#)]
70. Vansteenberge, S.; Verheyden, S.; Cheng, H.; Edwards, L.R.; Keppens, E.; Claeys, P. Paleoclimate in continental northwestern Europe during the Eemian and Early-Weichselian (125–97 ka): Insights from a Belgian speleothem. *Clim. Past Discuss.* **2016**, *12*, 1455–1458.
71. Wainer, K.; Genty, D.; Blamart, D.; Daëron, M.; Bar-Matthews, M.; Vonhof, H.; Dublyansky, Y.; Pons-Branchu, E.; Thomas, L.; Van Calsteren, P.; et al. Speleothem record of the last 180 ka in Villars cave (SW France): Investigation of a large $\delta^{18}\text{O}$ shift between MIS6 and MIS5. *Quat. Sci. Rev.* **2011**, *30*, 130–146. [[CrossRef](#)]
72. Stroeven, A.P.; Hättestrand, C.; Kleman, J.; Heyman, J.; Fabel, D.; Fredin, O.; Goodfellow, B.W.; Harbor, J.M.; Jansen, J.D.; Olsen, L.; et al. Deglaciation of Fennoscandia. *Quat. Sci. Rev.* **2016**, *147*, 91–121. [[CrossRef](#)]
73. Alexanderson, H.; Eskola, K.; Helmens, K. Optical Dating of a Late Quaternary Sediment Sequence from Sokli, Northern Finland. *Geochronometria* **2008**, *32*, 51–59. [[CrossRef](#)]
74. Helmens, K.; Johansson, P.; Räsänen, M.; Alexanderson, H.; Eskola, K. Ice-free intervals continuing into Marine Isotope Stage 3 at Sokli in the central area of the Fennoscandian glaciations. *Bull. Geol. Soc. Finl.* **2007**, *79*, 17–39. [[CrossRef](#)]
75. Mokeddem, Z.; McManus, J.F.; Oppo, D.W. Oceanographic dynamics and the end of the last interglacial in the subpolar North Atlantic. *Proc. Natl. Acad. Sci. USA* **2014**, *111*, 11263–11268. [[CrossRef](#)]



© 2019 by the authors. Licensee MDPI, Basel, Switzerland. This article is an open access article distributed under the terms and conditions of the Creative Commons Attribution (CC BY) license (<http://creativecommons.org/licenses/by/4.0/>).